

Localized Nonlinear Solution Strategies for Efficient Simulation of Unconventional Reservoirs

Jiamin Jiang

Chevron Energy Technology Co.

1500 Louisiana St., Houston, TX 77002, USA

Abstract

Accurate and efficient numerical simulation of unconventional reservoirs is challenging. Long periods of transient flow and steep potential gradients occur due to the extreme conductivity contrast between matrix and fracture. Detailed near-well/near-fracture models are necessary to provide sufficient resolution, but they are computationally impractical for field cases with multiple hydraulic-fracture stages.

Previous works in the literature of unconventional simulations mainly focus on the gridding level that adapts to wells and fractures. Limited research has been conducted on nonlinear strategies that exploit locality across timesteps and nonlinear iterations. It was reported that an individual Newton update is typically sparse and nonlinear convergence is constrained by a small portion of the model. To perform localized computations, an *a-priori* strategy is essential to first determine the active subset of simulation cells for the subsequent iteration. The active set flags the cells that will be updated, and then the corresponding localized linear system is solved.

The objective of this work is to develop localization methods that are readily applicable to complex fracture networks and flow physics in unconventional reservoirs. By utilizing the diffusive nature of pressure updates, an adaptive algorithm is proposed to make adequate estimates for the active domains. In addition, we further develop a localized solver based on nonlinear domain decomposition (DD). Compared to a standard DD method, domain partitions are dynamically constructed. The new solver provides effective partitioning that adapts to flow dynamics and Newton updates.

We evaluate the developed methods using several complex problems with discrete fracture networks. The problems consider multi-phase and compositional fluid systems with phase changes. The results show that large degrees of solution locality present across timesteps and iterations. Compared to a standard Newton solver, the new solvers enable superior computational performance. Moreover, Newton convergence behavior is preserved, without any impact on solution accuracy.

1. Introduction

Unconventional reservoirs have received great attention as a primary energy resource in the past decade worldwide. Economic production from these reservoirs depends on effective stimulation by means of hydraulic fracturing. Micro-seismic measurements and other evidence suggest the creation of complex fracture networks that connect huge reservoir surface areas to the wellbore [1-3]. In terms of reservoir development and management, numerical simulation continues to play a critical role in evaluating and optimizing the stimulation and production processes [4,5].

*Corresponding author

Email address: jiamin.jiang@chevron.com (Jiamin Jiang)

Because of the ultra-low permeability of matrix, a long period of transient flow occurs in unconventional formation. The extreme contrast in conductivity between matrix and fracture also results in steep potential gradients that are difficult to capture. Therefore, detailed near-well/near-fracture models are necessary to provide sufficient resolution for the matrix-fracture interactions [3,4,6]. However, a fine grid simulation requires too much CPU time and it is impractical to perform for the entire domain in field cases with multiple hydraulic-fracture stages [5,7,8].

Several modeling approaches for fractured-well have been proposed in the literature, attempting to improve the solution efficiency while maintaining the accuracy. One simple approach is applying local grid refinement (LGR) on a coarse background grid [4,8-14]. A number of meshing algorithms are available to generate adaptive and optimized mesh with good quality around discrete fractures. Pruess and Narasimhan [15] developed a sub-gridding method called multiple interacting continua (MINC) by subdividing each matrix cell according to the distance from fractures. The MINC method is intended to improve the classical dual-porosity model [16,17], and subsequently better characterize the transient effects with sharp solution gradients. In recent years, MINC was widely applied and extended for the simulations of unconventional reservoirs [12, 18-23]. In addition, Ding et al. [7] proposed a coupled modeling method that combines a coarse-grid reservoir model with detailed near-fracture models. The two models are solved, and the associated boundary conditions are updated in an alternate mode. The coupled method can be viewed as dynamic upscaling that computes the time-dependent fracture index for the coarse domain. Although some promising results were presented, the detailed models may still take a large fraction of the overall computational expense.

In reservoir simulation, the Fully Implicit Method (FIM) is often used for the temporal discretization of the conservation equations [24,25]. FIM offers unconditional stability, but it requires the solution of large coupled nonlinear systems. For a target timestep, a sequence of Newton iterations is performed until convergence. This iterative process is expensive and can account for a significant fraction of the total cost. Here define n as the total number of degrees of freedom in a system. Considering the costs of computing the residual vector, Jacobian matrix, and thermodynamic properties, the overall complexity of a nonlinear iteration is generally superlinear in n [26]. Recently, an algebraic dynamic multilevel method (ADM) was introduced for fully implicit simulations of flow and transport in heterogeneous porous/fractured media [13,27,28]. Built on the fine-scale FIM discrete system, ADM constructs a multilevel FIM system on a dynamic nested grid. The test results showed that ADM provided accurate solutions by employing only a fraction of the fine-scale grid-cells.

Previous works in the literature of unconventional simulations mainly focus on the gridding level that adapts to wells and fractures. Limited research has been conducted on solver techniques that exploit locality across timesteps and nonlinear iterations. The benefit of this type of methods is evident: the solution accuracy is maintained, because neither discretization scheme nor spatial mesh will be modified [26,29]. Simulation studies have shown that flow dynamics evolve quite slowly within the ultra-tight formation. Pressure drop may remain in the vicinity of fractures even after years of production [4,7,20]. Conceivably, a significant speedup can be achieved if performing adaptive computations only for the locales that are undergoing changes. In addition to the timestep level, a large degree of locality also presents on the nonlinear (Newton) level. It was reported that an individual Newton update is typically sparse and the nonlinear convergence is constrained by a small portion of the model [26,29,30]. To exploit the locality at each iteration, an *a-priori* strategy is essential to first identify the active subset of simulation cells. The active set flags the cells that will be updated, and then the corresponding localized linear system is solved. Lu and Beckner [30] observed that over the course of several iterations, the sparsity pattern of the Newton updates was related to that of the discrete residual vector. They proposed to use non-zero entries in the residual vector as an estimate of the active set for the subsequent iteration. It should be mentioned that

their heuristic strategy may suffer from an efficiency issue due to overly conservative estimate. Sheth and Younis [29] have shown that missing any non-zero update during the localization process may lead to worse nonlinear convergence, compared to the standard Newton method. A theoretical framework was then developed to predict the sparsity pattern of Newton updates. Analytical derivations were made to ensure a conservative estimate of the active sets. The results in Sheth and Younis [29] demonstrated that their localization method performs quite well for several challenging models.

In this work we do not intend to rely on an analytical derivation or conservative estimate for the active sets. The objective is to develop localization methods that readily accommodate to complex fracture networks and flow physics for the simulations of unconventional reservoirs. Through aggressive localization, the computational speedup is expected to be greatly improved. We recently revealed that the Newton updates for pressure-driven problems exhibit diffusive and global behaviors, because of its parabolic nature [31]. By utilizing the nature of pressure updates, an adaptive algorithm is proposed to make adequate estimates for the active domains. In addition, we further develop a localized solver based on nonlinear domain decomposition (DD). Compared to a standard DD method, domain partitions are dynamically constructed from the previous iterations. During the nonlinear DD process, the subproblems of an iteration are solved sequentially, and thus the localization can be naturally achieved. This leads to a reliable strategy that exploits the locality while preserving the convergence behavior of the standard Newton process. Note that the two methods developed involve different complexities and efforts for implementation. Subsequently, their applications depend on specific efficiency and implementation considerations.

We evaluate the localization methods using several complex problems with discrete fracture networks. The test problems consider multi-phase and compositional fluid systems with phase changes. The results show that large degrees of solution locality present across timesteps and iterations. Compared to a standard Newton solver, the new solvers exhibit superior computational performance. Moreover, Newton convergence behavior is preserved, without any impact on the solution accuracy.

2. Isothermal compositional model

We consider compressible gas-oil flow in porous media without capillarity. We ignore water that does not exchange mass with the hydrocarbon phases.

The conservation equations for the isothermal compositional problem containing n_c components are written as,

$$\frac{\partial}{\partial t} [\phi (x_c \rho_o s_o + y_c \rho_g s_g)] + \nabla \cdot (x_c \rho_o \mathbf{u}_o + y_c \rho_g \mathbf{u}_g) - q_c = 0, \quad (1)$$

where $c \in \{1, \dots, n_c\}$. x_c and y_c are molar fractions of component c in the oil and gas phases, respectively. ϕ is rock porosity and t is time. ρ_l is phase molar density. s_l is phase saturation. q_c is well flow rate.

Phase velocity \mathbf{u}_l is expressed as a function of phase potential gradient $\nabla \Phi_l$ using the extended Darcy's law,

$$\mathbf{u}_l = -k \lambda_l \nabla \Phi_l = -k \lambda_l (\nabla p - \rho_l g \nabla h). \quad (2)$$

where k is rock permeability. p is pressure. Capillarity is assumed to be negligible. g is gravitational acceleration and h is height. Phase mobility is given as $\lambda_l = k_{rl} / \mu_l$. k_{rl} and μ_l are relative permeability and viscosity, respectively.

In order to close the nonlinear system, additional equations are needed. These include the thermodynamic equilibrium constraints,

$$f_{c,o}(p, \mathbf{x}) - f_{c,g}(p, \mathbf{y}) = 0, \quad (3)$$

where p , T , and z_c denote pressure, temperature, and overall molar fraction, respectively. $f_{c,l}$ is the fugacity of component c in phase l .

We now write the phase constraints,

$$\sum_{c=1}^{n_c} x_c - 1 = 0, \quad \sum_{c=1}^{n_c} y_c - 1 = 0, \quad (4)$$

and the saturation constraint as,

$$s_o + s_g - 1 = 0. \quad (5)$$

The above system of equations provide a complete mathematical statement for two-phase multi-component flow. The local equilibrium constraints are enforced only when both phases are present.

3. Natural-variables formulation

An important aspect of any compositional formulation is the choice of dividing the equations and unknowns into primary and secondary sets. Here we employ the popular natural-variables set [25,32]. The primary unknowns include pressure, saturations, and molar fractions,

- (1) p – pressure [1],
- (2) s_l – phase saturations [2],
- (3) x_c, y_c – phase compositions of each component [$2n_c$].

The size of each variable is given in square bracket.

The various coefficients can be obtained as functions of the base variables. For a two-phase cell, the molar phase fraction is related to saturation as follows,

$$\nu_l = \frac{\rho_l s_l}{\sum_m \rho_m s_m} \quad (6)$$

and overall molar fraction of component c is written as,

$$z_c = x_c \nu_o + y_c \nu_g \quad (7)$$

Note that for single-phase (l) mixture, $\nu_l = s_l = 1$, and $x_{c,l} \equiv z_c$.

3.1. Variable substitution

An essential ingredient of the natural-variables formulation is the ‘variable substitution’ process [32]. A common strategy for variable-switching between Newton iterations during a timestep is,

1. For any cell whose status in the previous iteration is single-phase, run the phase stability test [33] to check if the mixture becomes two-phase. For the mixture that splits into two phases, perform the flash to compute the phase compositions [34].

2. If a cell is already in the two-phase state, the thermodynamic constraints are included in the nonlinear system as part of the global Jacobian.

3. If a phase saturation, or phase fraction, becomes negative between two successive iterations, the phase disappears, and appropriate variable-switching is performed.

The system of conservation equations is solved for single-phase regimes, and the combination of conservation equations and thermodynamic constraints is solved for the two-phase regime.

3.2. Phase behavior

Phase behavior computation is usually a stand-alone procedure for detecting phase changes. For a mixture of n_c components and two phases, the mathematical model describing the thermodynamic equilibrium is [32],

$$f_{c,o}(p, \mathbf{x}) - f_{c,g}(p, \mathbf{y}) = 0, \quad (8)$$

$$z_c - \nu_o x_c - (1 - \nu_o) y_c = 0, \quad (9)$$

$$\sum_{c=1}^{n_c} (x_c - y_c) = 0. \quad (10)$$

where ν_l is molar fraction of phase l . We assume that p , T , and z_c are known. The objective is to find all the x_c , y_c and ν_l .

Phase behavior of a hydrocarbon mixture is commonly described using an Equation of State (EoS) model.

4. Nonlinear solution strategies

The spatial and temporal discretization schemes used for the compositional flow model are summarized in Appendix A.

4.1. Newton method

At each timestep of a FIM simulation, given the current state u^{n_t} , and a fixed timestep size Δt , we seek to obtain the new state u^{n_t+1} .

The nonlinear residual system is solved by the Newton method,

$$F(u^{n_t+1}) = 0 \quad (11)$$

The Newton method generates a sequence of iterates, u^ν , $\nu = 0, 1, \dots$, each involving the construction of a Jacobian matrix and solution of the resulting linear system,

$$J(u^\nu) \delta u^\nu = -F(u^\nu) \quad (12)$$

where

$$\delta u^\nu = u^{\nu+1} - u^\nu \quad (13)$$

and $J(u) = \frac{\partial F}{\partial u}(u)$ denotes the Jacobian matrix of F with respect to u .

Here we assume that entries of Newton update such that $|\delta u_i| < \epsilon$ are essentially negligible. Given a Newton iteration, the support set is defined for the indices of cells that exhibit non-zero update,

$$\text{supp } \delta u = \{i: |\delta u_i| \geq \epsilon, i = 1, \dots, n\} \quad (14)$$

4.2. Locality within solution processes

In this work we focus on the solution process for the pressure-driven production problem with multi-phase multi-component fluid. We aim to exploit two levels of locality for improving computational efficiency. The first is on the timestep level. Because of the ultra-low matrix permeability in unconventional formation, transient flow within matrix may last a long period. As a result, flow dynamics (e.g. pressure propagation) evolve slowly and locally. During early stage of production, only a small portion of domain undergoes considerable variable changes.

For a timestep, the solution update is the sum of all the corresponding Newton updates. Conceivably, the locality also presents on the nonlinear (Newton) level, even if

most of the domain is affected over the timestep. Previous works showed that an individual update computed for flow and transport problem is typically sparse and constrained by a small subset of cells [26,29,30].

Here we show an example with two-fracture to demonstrate the solution behavior. The details of the model will be given in the result section. The flagging profiles for the Newton iterations of a timestep are plotted in **Fig. 1**. The cells that exhibit non-zero pressure updates are flagged in color blue. As we can see, the first iteration reaches the maximum area, and the region gets smaller as the iterations proceed. In the last iteration, the support set of the updates localizes to just a few cells.

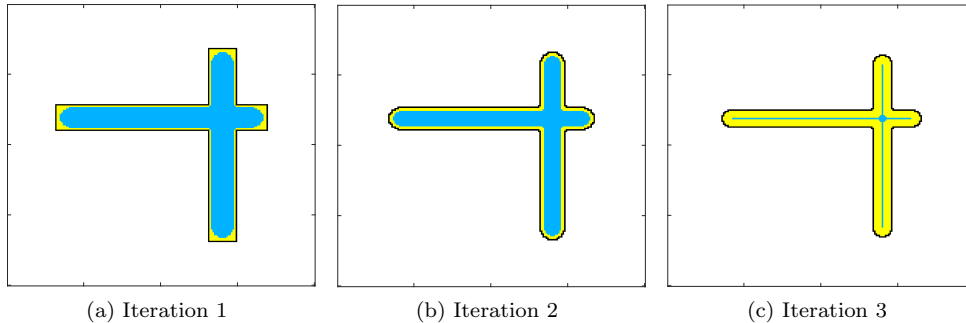


Figure 1: Flagging of the pressure updates for the three Newton iterations of a timestep.

Lu and Beckner [30] proposed an adaptive Newton strategy that solves localized systems. Their method identifies unconverged cells and their neighbors as the active subset to be updated. The unconverged set is inflated to a heuristic extent (e.g. plus one layer of neighbor cells), as a safety measure.

From the simulation studies, we also observe that under a convergent Newton sequence, the support set of updates always shrinks after each iteration, such that,

$$\text{supp } \delta u^{\nu+1} \subseteq \text{supp } \delta u^{\nu} \quad (15)$$

Therefore, the support set from a current Newton iteration becomes an adequate estimate for the subsequent iteration.

The adaptive algorithm by Lu and Beckner [30] is simple to implement. However, the algorithm starts with the entire domain at the first iteration of a timestep, to ensure conservative estimates for the active set. This will considerably contribute to the overall computational cost.

Our recent studies revealed that Newton iterations are closely tied to the underlying physics problem [31]. The updates for a hyperbolic transport problem may have local support that propagates through the domain as the Newton process goes forward. By comparison, the support of a pressure (flow) problem shows diffusive and global behaviors, due to its parabolic nature. To exploit this mechanism, here we propose a localized Newton strategy, which is aggressive in the way that it does not require an initial conservative estimate for the active domain. We observe that the support of pressure updates tends to reach the solution front at the first iteration. Therefore, the localized algorithm can start with a moderate active domain Ω_A , and expand it if necessary using the outermost (boundary) layer of Ω_A .

4.3. Localized Newton algorithm

We describe the algorithm based on the proposed localized Newton strategy. Consider a nonlinear system of equations $F = (F_1, \dots, F_n)^T$ with unknowns $u = (u_1, \dots, u_n)^T$. Let $V = (1, \dots, n)$ be an index set; i.e., there is one integer for each F_i and unknown u_i . Let V_A be the index set that contains the active cells, and n_A be the dimension of V_A . We

define $V_B \subseteq V_A$ as the cell set for the outermost (boundary) layer of the active domain. Further define the set $V_{nbr}^{i,m}$ for the neighbors of cell i , and m is the number of layers that are incorporated. The illustration for $V_{nbr}^{i,m}$ with $m = 1$ and $m = 2$ is plotted in **Fig. 2**. The neighbor cells are flagged in yellow.

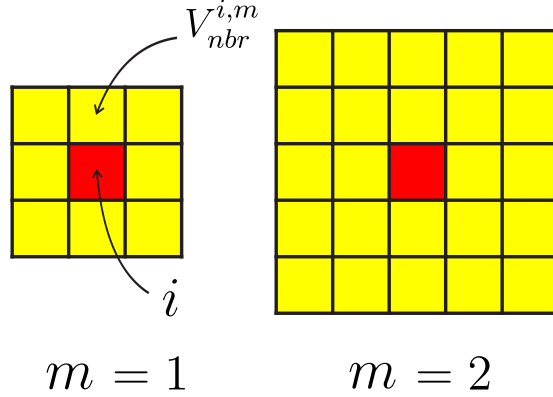


Figure 2: Illustration for the neighbors of cell i .

Let R_A be a Boolean matrix of dimension $n_A \times n$. R_A corresponds to the restriction operator from V to V_A . The transpose matrix R_A^T is an extension operator from V_A to V . Then the nonlinear function and the local unknowns of the active set V_A can be expressed as $F_A = R_A F$ and $u_A = R_A u$, respectively. The Jacobian of F_A is,

$$J_A = R_A J R_A^T \quad (16)$$

Note that the submatrix J_A can be directly constructed, and thus the full matrix J is never required. There is no need to evaluate the cell properties, residual and Jacobian for the inactive domain.

The localization method takes as input a state at time level n_t and outputs the updated state. The algorithmic details can be described as,

- Step 1. Set the iteration counter ν to zero, and initialize u^ν to the current state u^{n_t} . Construct the initial active set V_A and the associated boundary set V_B .
- Step 2. Perform localization: solve the reduced linear system over the active domain, and update the solution.
- Step 3. For each cell i in V_B , if the update is larger than the cutoff value, inflate V_A with the neighbor subset $V_{nbr}^{i,m}$.
- Step 4. If there is any non-negligible update in V_B , the localization status stays in the ‘expand’ mode; otherwise, switch to the ‘shrink’ mode, and V_A is specified as the support set of δu_A .
- Step 5. Check convergence criteria of Newton iterations. If not converged, go back to Step 2. Otherwise, the timestep is finished.

The proposed method is also outlined in Algorithm 1. We can see that the localization process determines the active set that needs to be solved for the subsequent iteration. The process consists of two stages. In the first stage, V_A does not fully cover the actual support of the timestep. Based on the diffusive nature of pressure updates, V_B is used to detect and expand the active domain. The localized algorithm is self-adaptive in a sense that Newton update already provides an adequate estimate.

The initial active set can be constructed to comprise the cells in the vicinity of wells or fractures. Subsequently, computational speedup will be greatly increased. On the

Algorithm 1 Localized Newton

```

1:  $\nu = 0$ ,  $u^\nu = u^{n_t}$ 
2: Initialize  $V_A$  and  $V_B$ .
3: while is_expand or not_converged do ▷ Newton loop
4:   Solve reduced linear system,
      $J_A \delta u_A = -F_A$ 
5:    $u^{\nu+1} = u^\nu + R_A^T \delta u_A$ 
6:   Check convergence criteria.
7:   for  $i \in V_B$  do ▷ Determine active set
8:     if  $|\delta u_{i,A}| \geq \epsilon$  then
9:       Obtain  $V_{nbr}^{i,m}$  of cell  $i$ ,
10:       $V_A = V_A \cup V_{nbr}^{i,m}$ 
11:     end if
12:   end for
13:   if  $\|\delta u_B\|_\infty < \epsilon$  then ▷ Shrink mode
14:     is_expand  $\leftarrow$  false
15:      $V_A = \text{supp } \delta u_A$ 
16:   else
17:     is_expand  $\leftarrow$  true
18:   end if
19:   Update  $V_B$  from  $V_A$ .
20:    $\nu \leftarrow \nu + 1$ 
21: end while

```

other hand, the iterations taken during the ‘expand’ mode may degrade the nonlinear convergence, compared to the standard Newton method. In practice, a balance needs to be achieved between more aggressive localization and increased number of iterations.

It should be noted that the iterative process for expanding active domain can be viewed as a nonlinear domain decomposition (DD) problem. Each subproblem is solved with Dirichlet boundary (constant pressure) conditions. Similarly to nonlinear preconditioning, the subdomain solutions can provide better initial guesses for Newton iterations. As a result, the localized solver shows satisfying convergence performance from the simulation cases.

4.4. Adaptive Nonlinear Domain Decomposition

For a localized Newton algorithm, more iterations may be required, if the estimate for the support set is not conservative. On the other hand, an excessively conservative estimate will reduce the speedup gained from the localized computations.

In this work we further develop an adaptive method that provides aggressive localization, while preserving the convergence behavior of the standard Newton process. To present the method, consider first a nonlinear domain decomposition (DD) with non-overlapping partitions,

$$\bigcup_{k=1}^N V_k = V, \quad V_j \cap V_k = \emptyset \text{ if } j \neq k, \quad \text{and } V_k \subset V. \quad (17)$$

Let n be the total number of unknowns and n_k be the total number of unknowns associated with the subset V_k . The restrictions of u and F to V_k are $u_k = R_k u$ and $F_k = R_k F$, respectively. The Jacobian of the subproblem k is given as,

$$J_k = R_k J R_k^T \quad (18)$$

with $k = 1, \dots, N$. The boundary conditions for a subproblem are Dirichlet-type and taken from the neighboring subdomains.

A global solution of the nonlinear DD method is obtained by solving first subproblems and then gluing them together [35],

$$u^{\nu+1} = \sum_{k=1}^N R_k^T u_k^{\nu+1} \quad (19)$$

It is common to apply the additive (Jacobi) form of the Schwarz methods. For a standard DD, static partitions of simulation grid are performed in a preprocessing step [35-37].

To exploit the localized behaviors of flow problems, we propose instead an adaptive DD solver based on dynamic partitions. Utilizing the diffusive nature of pressure updates, subdomains are constructed from the previous iterations. To achieve localized computations, the subproblems of a nonlinear DD iteration are solved sequentially. This leads to a multiplicative (Gauss-Seidel) Schwarz method.

The algorithmic details of the adaptive DD method for a timestep are given as,

- Step 1. Set the iteration counters ν and k to zero, and initialize u^ν to the current state u^{n_t} . Construct the initial active set V_A^k , and the associated boundary sets V_B^k and $V_{\partial B}^k$. Define ∂B as the outer layer adjacent to Ω_A , such that $V_{\partial B}^k \cap V_A^k = \emptyset$.
- Step 2. Start expanding the active domain, and perform localized computations. Construct the subdomains, and the associated cell sets, using the Newton updates. Specifically, for each cell i in V_B^k , if the update is larger than the cutoff value, inflate V_A^{k+1} and the total active set V_T with the neighbor subset $V_{nbr}^{i,m}$.
- Step 3. If there is any non-negligible update in V_B^k , remain in the ‘expand’ mode, and obtain the boundary sets of V_A^{k+1} . Otherwise, switch to the ‘shrink’ mode, indicating that the maximum support set over the timestep is reached.
- Step 4. Set N as the number of the constructed subdomains. Start the nonlinear DD loop, with the counter ν denoting the outer iteration. For each k , first collect $\delta u_{\partial B}^k$ over $V_{\partial B}^k$, from the latest Newton updates.
If there is any non-negligible element in $\delta u_A^{k,\nu}$ or $\delta u_{\partial B}^k$, perform localized computation and update the solution.
- Step 5. Check convergence criteria. Repeat the outer iteration until all the subdomains are converged.

The new adaptive solver is also outlined in Algorithm 2. Note that a subdomain needs to be solved only when the solution is not yet converged or the boundary values change. Therefore the localization is naturally achieved during the nonlinear DD process. This leads to a reliable strategy to exploit the locality for each outer iteration.

An outer iteration of the DD method can be written in a fixed-point form,

$$u^{\nu+1} = \sum_{i=1}^N R_i^T G_i(u^\nu) =: \mathcal{G}(u^\nu) \quad (20)$$

where the solution operator for a subproblem is,

$$u_{\Omega_i}^{\nu+1} = G_i(u^\nu) \quad (21)$$

As can be seen, evaluation of the function $\mathcal{G}(u)$ involves the solution of all the subproblems $(1, \dots, N)$. Despite its simple form, the fixed-point method may suffer from slow convergence, or even divergence [35,37]. Recently we proposed several ways of accelerating the nonlinear DD process [38]. The nonlinear acceleration techniques greatly improve the outer convergence behavior, while requiring little additional cost. The investigation on the outer convergence of the adaptive DD solver is subject to future work.

Algorithm 2 Adaptive Nonlinear Domain Decomposition

```

1:  $\nu = 0, k = 0$ 
2:  $u^\nu = u^{n_t}$ 
3: Initialize  $V_A^k, V_B^k$  and  $V_{\partial B}^k$ .
4:  $V_T = V_A^k$ 
5: while is_expand do ▷ Newton loop
6:   Local solve over  $V_A^k$ ,
      $J_A \delta u_A = -F_A$ 
7:    $u^{\nu+1} = u^\nu + R_A^T \delta u_A$ 
8:    $V_A^{k+1} \leftarrow \{\}$ 
9:   for  $i \in V_B^k$  do ▷ Determine active set
10:    if  $|\delta u_{i,A}| \geq \epsilon$  then
11:      Obtain  $V_{nbr}^{i,m}$  of cell  $i$ ,
12:       $V_T = V_T \cup V_{nbr}^{i,m}$ 
13:       $V_A^{k+1} = V_A^{k+1} \cup V_{nbr}^{i,m}$ 
14:    end if
15:  end for
16:  if  $\|\delta u_B\|_\infty < \epsilon$  then ▷ Shrink mode
17:    is_expand  $\leftarrow$  false
18:  else
19:    is_expand  $\leftarrow$  true
20:    Obtain  $V_B^T$  of  $V_T$ ,
21:     $V_B^{k+1} = V_B^T \cap V_A^{k+1}$ 
22:    Obtain  $V_{\partial B}^{k+1}$  of  $V_A^{k+1}$ .
23:  end if
24:   $k \leftarrow k + 1$ 
25: end while
26:  $N = k$ 
27:  $k = 0, \nu = 1$ 
28: while not_converged do ▷ Nonlinear DD loop
29:   for  $k < N$  do
30:    Collect  $\delta u_{\partial B}^k$  over  $V_{\partial B}^k$ .
31:    if  $\left\| \delta u_A^{k,\nu} \right\|_\infty \geq \epsilon$  or  $\left\| \delta u_{\partial B}^k \right\|_\infty \geq \epsilon$  then
32:      Local solve over  $V_A^k$ ,
33:       $u^{\nu+1} = u^\nu + R_A^T \delta u_A$ 
34:      Check convergence criteria.
35:    end if
36:  end for
37:   $\nu \leftarrow \nu + 1$ 
38: end while

```

5. Results

We evaluate the efficacy of the localization methods using several problems with discrete fracture networks. The problems include an oil-water system and a compositional system with phase changes. A 2D synthetic model is generated to contain a single-stage hydraulically-fractured horizontal well at the center of a reservoir. The fractures are assumed to fully penetrate the formation. An embedded discrete fracture model (EDFM) is employed to explicitly describe the discrete fractures. Lee et al. [39], Li and Lee [40], Hajibeygi et al. [41] and Moïnfar et al. [42] introduced and extended EDFM, which does not require simulation grid to conform to fracture geometry. Recent works on the implementations of EDFM for various types of problems include [8,12-14,43-48].

A simple time-stepping strategy is employed: starting with a small initial value, timestep sizes gradually increase to the maximum value. Newton convergence is based on the following criterion: solution (pressure) delta (increment) $\|\delta p\|_\infty < \epsilon_p$ between iterations. The specification of the base model is given in Table 1.

Table 1: Specification of the synthetic base model.

Parameter	Value	Unit
Initial pressure	2500	psi
Matrix porosity	0.05	
Rock compressibility	3.4e-4	1/psi
Matrix permeability	1e-19	m ²
Fracture permeability	1e-10	m ²
Fracture aperture	1e-3	m
Production BHP	1000	psi
Total simulation time	1500	day
Max timestep size	100	day

5.1. Grid sensitivity

We first test a $100\text{m} \times 100\text{m}$ model with two fractures to demonstrate the effect of transient flow. Initial water saturation is set as the connate saturation, so that water is immobile during simulations. Newton tolerance has the value of $\epsilon_p = 0.3$ psi. Simulations are run for three different levels of grid resolution.

Pressure profiles at the end of simulation are shown in **Fig. 3**. Oil rates are plotted in **Fig. 4**. As we can see, oil productions are largely underestimated by the coarse grid systems. The large cell sizes of coarse grid are not adequate for the sharp pressure variations in the vicinity of the fractures. On the other hand, the fine-grid case involves a large number of cells and thus requires significant computational efforts.

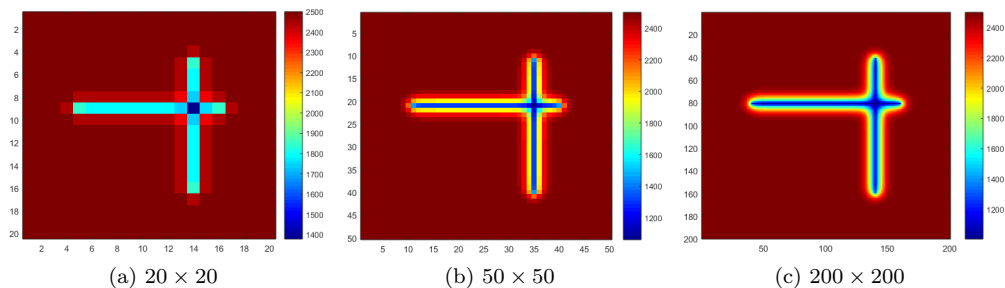


Figure 3: Pressure profiles for the three levels of grid resolution.

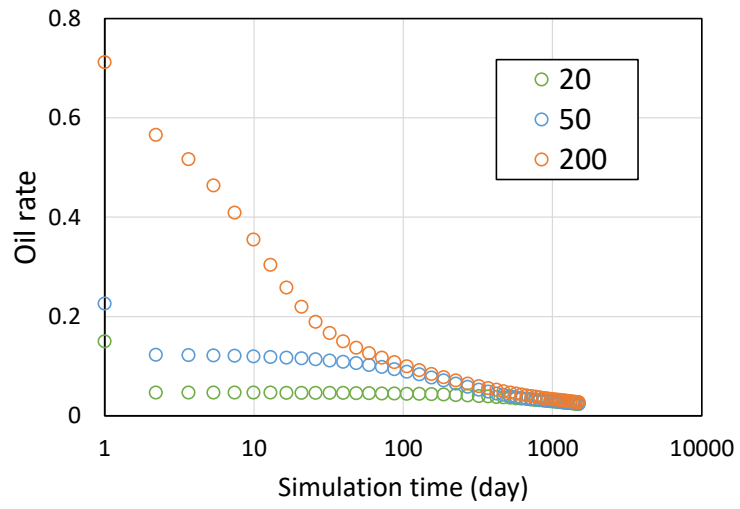


Figure 4: Oil rates for the three levels of grid resolution.

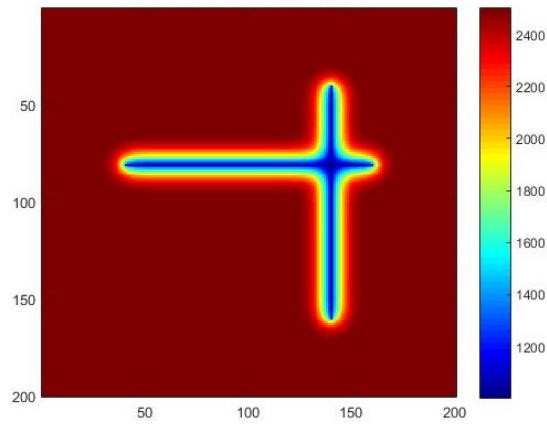


Figure 5: Pressure profile of Case 1.

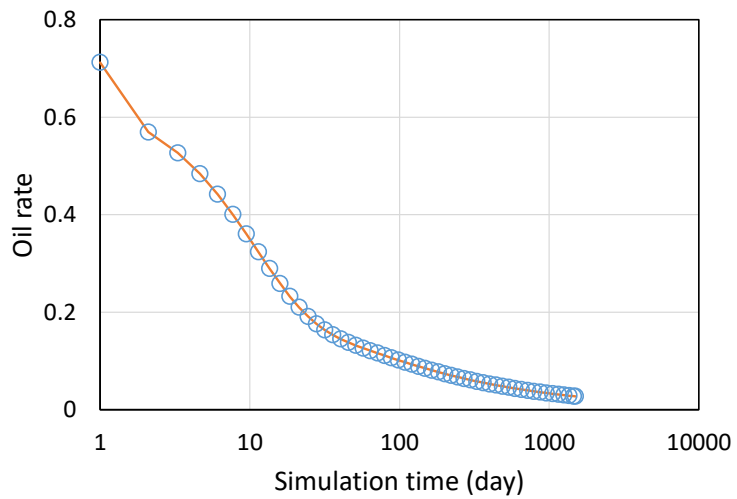


Figure 6: Oil rates of Case 1.

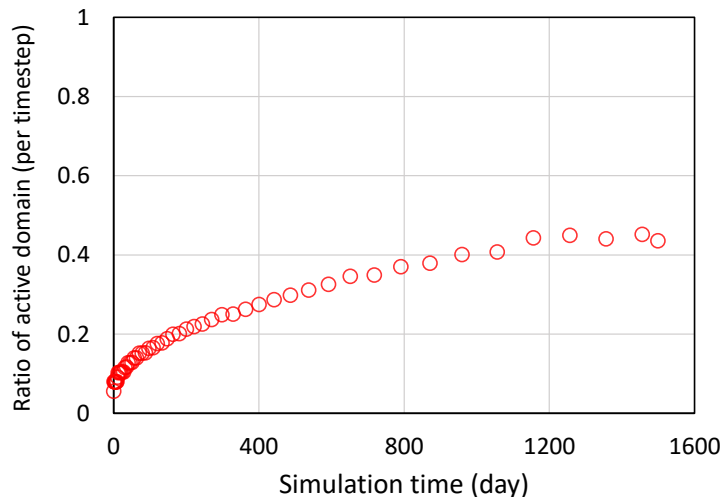


Figure 7: Ratios of active domain (per timestep) for Case 1.

5.2. Localized Newton method

5.2.1. Case 1

We test the model with 200×200 grid level. At every iteration, the localized Newton algorithm 1 provides the active set to be updated, and then solves the reduced linear system. Convergence tolerance of $\epsilon_p = 0.3$ psi is employed as the cutoff value for the active and boundary sets. The neighbor set $V_{nbr}^{i,m}$ with $m = 2$ is used to expand active domain. The support set of the last timestep is taken as the initial active set for the current timestep.

Pressure profile is shown in **Fig. 5**. We can observe that only a small fraction of the cells around the fractures undergoes significant changes of pressure. Oil rates are plotted in **Fig. 6**. As expected, the solution from the localization method exactly matches the reference solution. This is because the iterative processes converge under the same convergence tolerance.

We plot the ratios of active domain (per timestep) versus simulation time in **Fig. 7**. Note that 2-4 iterations are taken at each timestep. Computational performance of Case 1 is summarized in Table 2. M_A is defined as the ratio of the active to full sets. For the standard Newton, the total ratio M_A is equal to the total iteration number, with the average ratio as 1.

The results show that the localization method exhibits good convergence performance. As we discussed before, the iterations for expanding active domain can be viewed as non-linear preconditioning which provides better initial guesses. The localized solver achieves an at least 13-fold reduction in computations, compared to the standard solver. The actual simulation speedup depends on the scaling of computational complexity $O(n^\beta)$.

Table 2: Computational performance of Case 1.

	Timesteps	Total iterations	Total ratio M_A	Average ratio M_A per iteration
Localized Newton	54	159	11.4	0.072
Standard Newton	54	156	156	1

We re-run the case using the localized Newton for one timestep with the size of 50 days. The timestep size is equal to the total simulation time. The profiles for the flagging of cells over the 4 iterations are plotted in **Fig. 9**. Four types of cell sets are specified:

1. active set (in color yellow); 2. boundary set (black); 3. the active cells with non-negligible update (the support set), (blue); and 4. the boundary cells with non-negligible update (red). A color illustration for the cell types is given in **Fig. 8**.

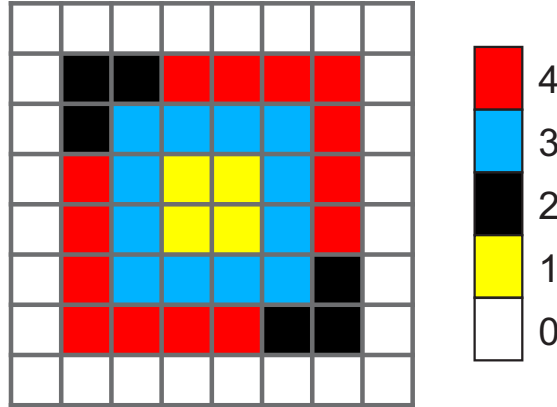


Figure 8: Illustration for the cell types: 1. active set (yellow); 2. boundary set (black); 3. the active cells with non-negligible update (blue); 4. the boundary cells with non-negligible update (red).

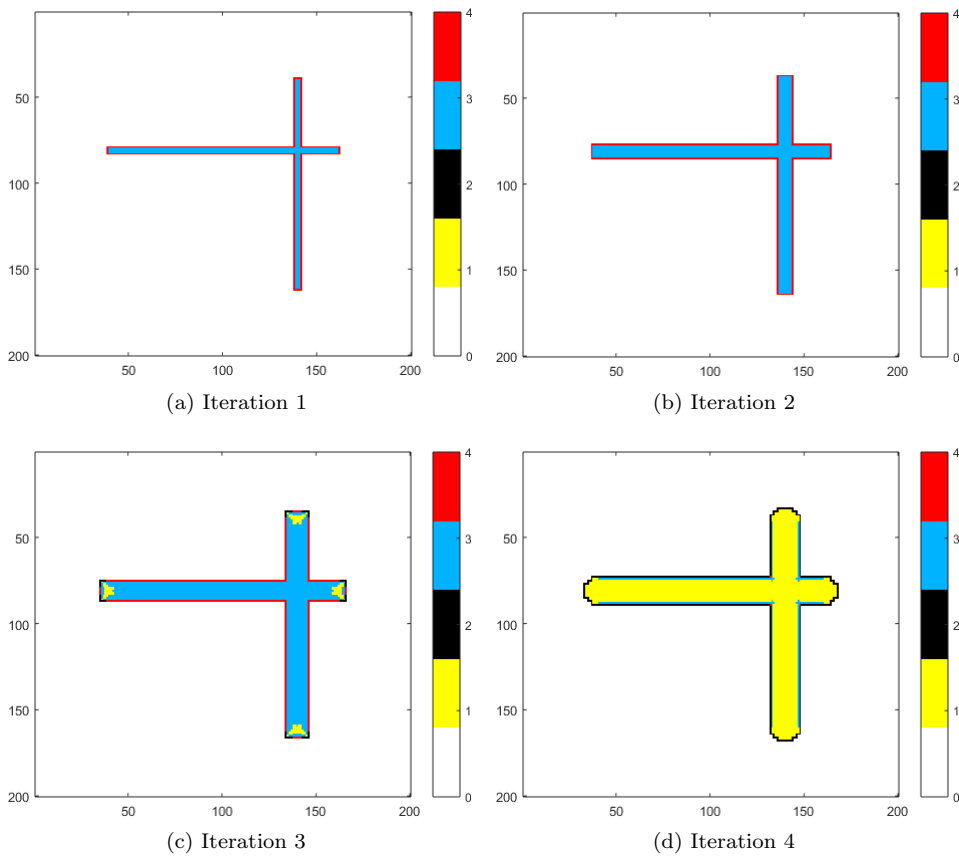


Figure 9: Flagging profiles for Case 1.

As can be seen, the initial active set is small and not conservative, resulting in aggressive localization and thus high computational speedup. As the iterations proceed, the active domain expands until the maximum area is reached.

5.2.2. Case 2

We test a $300\text{m} \times 300\text{m}$ model with 200×200 grid and a more complex fracture network. The model contains 4 secondary fractures with permeability of $1\text{e-}13 \text{ m}^2$. Pressure profile is shown in **Fig. 10**. We plot the ratios of active domain (per timestep) versus simulation time in **Fig. 11**.

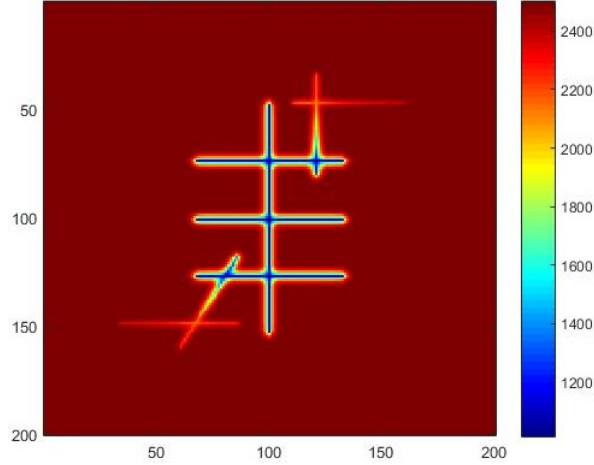


Figure 10: Pressure profile of Case 2.

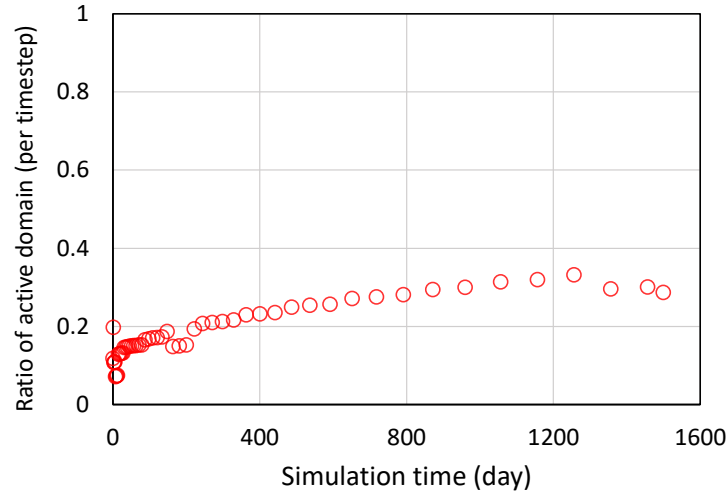


Figure 11: Ratios of active domain (per timestep) for Case 2.

Computational performance of Case 2 is summarized in Table 3. From the results we see that the localization method enables a significant reduction in computations, while preserving the original convergence behavior.

Table 3: Computational performance of Case 2.

	Timesteps	Total iterations	Total ratio M_A	Average ratio M_A per iteration
Localized Newton	54	155	10.1	0.065
Standard Newton	54	153	153	1

We re-run the case for one timestep with the size of 50 days. The profiles for the

flagging of cells over the 4 iterations are plotted in **Fig. 12**. The color illustration of cell sets is the same as specified in the previous section. As can be seen, the sparsity patterns of the updates vary largely from one iteration to the next. After two iterations, the nonlinear convergence is constrained to just several cells.

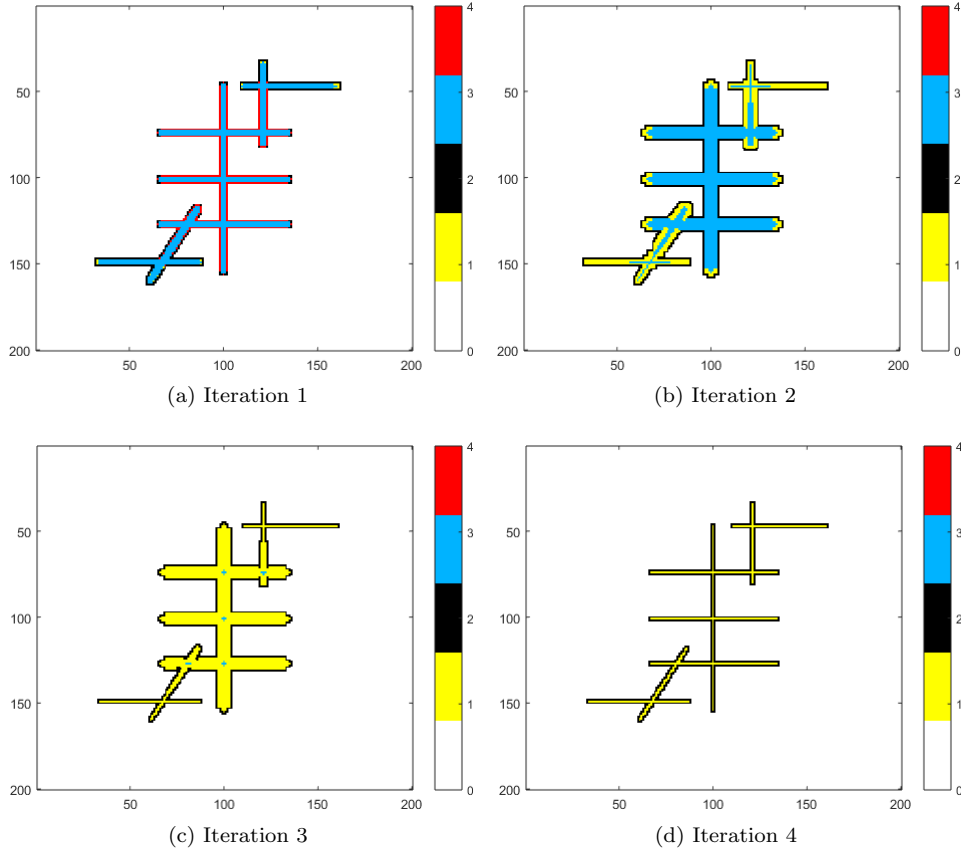


Figure 12: Flagging profiles for Case 2.

5.2.3. Case 3

We again consider the model from Case 2, but with 100×100 grid. The model uses a two-component fluid system where the initial oil is made of $\{C_1(50\%), C_{10}(50\%)\}$. Phase density and viscosity depend on pressure and compositions. Phase molar density ρ_l is evaluated based on the compressibility (Z) factor from the PR EoS. Phase viscosity μ_l is computed by the correlation of Lohrenz et al. [49]. Simple relative permeabilities given by quadratic function are used. Initial pressure is 2900 psi and temperature is 340 K. The total simulation time is 500 days, with the maximum timestep size as 50 days. The other parameters in the previous case remain unchanged.

The profiles for phase status and gas saturation are shown in **Fig. 13** and **Fig. 14**, respectively. As pressure drops below the bubble-point, gas appears around the fractures. The transient effects of saturation and phase dynamics can be difficult to capture using coarse grid. From the results we observe that the saturation updates exhibit considerable locality. By comparison, the pressure updates affect a much larger region.

We plot the ratios of active domain (per timestep) versus simulation time in **Fig. 15**. Computational performance of Case 3 is summarized in Table 4. The localized Newton method shows superior performance, with a small increase of iterations.

It should be noted that the ratio M_A may increase with a larger portion of the domain taken by fracture networks. We do not exploit solution locality for fractures

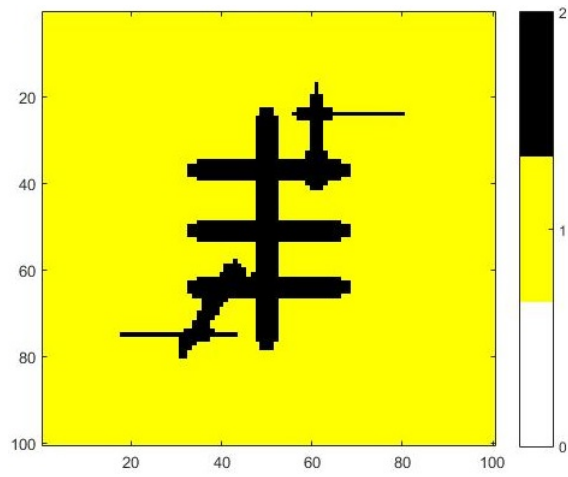


Figure 13: Phase status of gas for Case 3.

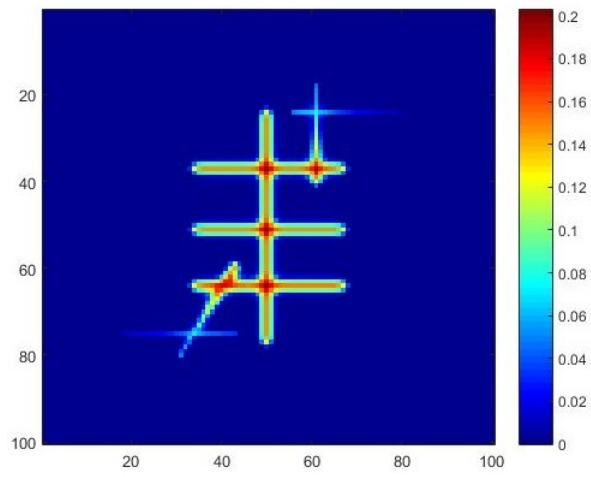


Figure 14: Gas saturation for Case 3.

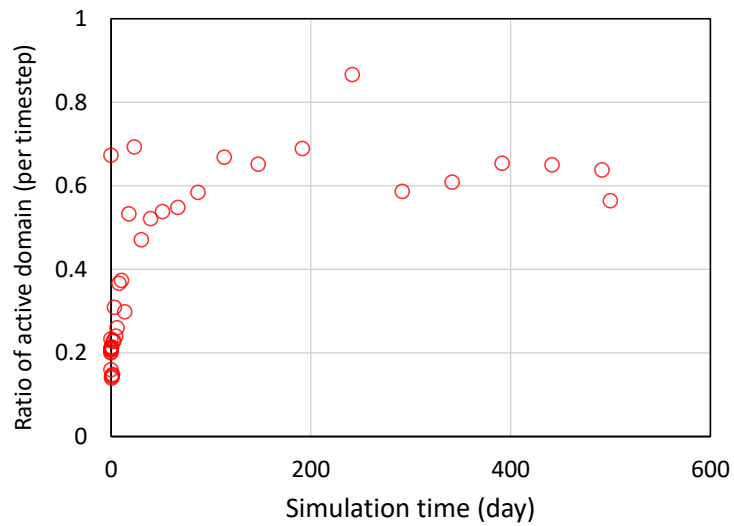


Figure 15: Ratios of active domain (per timestep) for Case 3.

under the current implementations. Overall computational efforts can be further reduced, if applying localization also to fracture cells. The localized solver will be more effective, for large fracture networks with various conductivities and secondary fractures, because of the transient effects in fracture cells.

Table 4: Computational performance of Case 3.

	Timesteps	Total iterations	Total ratio M_A	Average ratio M_A per iteration
Localized Newton	40	153	16.1	0.1
Standard Newton	40	148	148	1

5.3. Adaptive Nonlinear DD method

We study the adaptive nonlinear DD (Algorithm 2) which is based on dynamic partitions to perform localized computations. The developed solver can make adequate estimates of the active set for each inner iteration.

5.3.1. Case 2.1

We use the same model as specified in Case 1. Computational performance of the case is summarized in Table 5. The adaptive DD solver greatly reduces the computational cost, while taking much more iterations. This is because each outer iteration consists of multiple inner iterations in the nonlinear DD process. We observe that the size of a subdomain system is relatively small and the total number of outer iterations is comparable to the standard Newton method. The ratios of active domain (per timestep) versus simulation time are plotted in **Fig. 16**.

Table 5: Computational performance of Case 2.1.

	Timesteps	Total (inner) iterations	Total ratio M_A	Average ratio M_A per iteration
Adaptive Nonlinear DD	54	804	20.8	0.026
Standard Newton	54	156	156	1

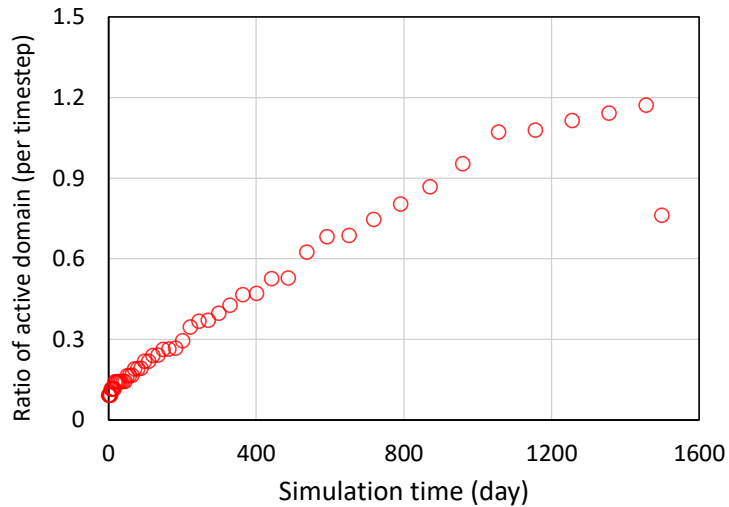


Figure 16: Ratios of active domain (per timestep) for Case 2.1.

We re-run the case for one timestep with the size of 50 days. The neighbor set $V_{nbr}^{i,m}$ is specified with $m = 4$. Flagging profiles of cells over the 4 iterations are plotted in **Fig. 17**. As we can see, the timestep converges after 2 outer iterations. The algorithm constructs the subdomains that adapt to the flow dynamics and pressure updates. During the nonlinear DD process, the subproblems are solved sequentially, to achieve localization. The results confirm that the support set of the timestep is contained in the union of all the flagged subsets.

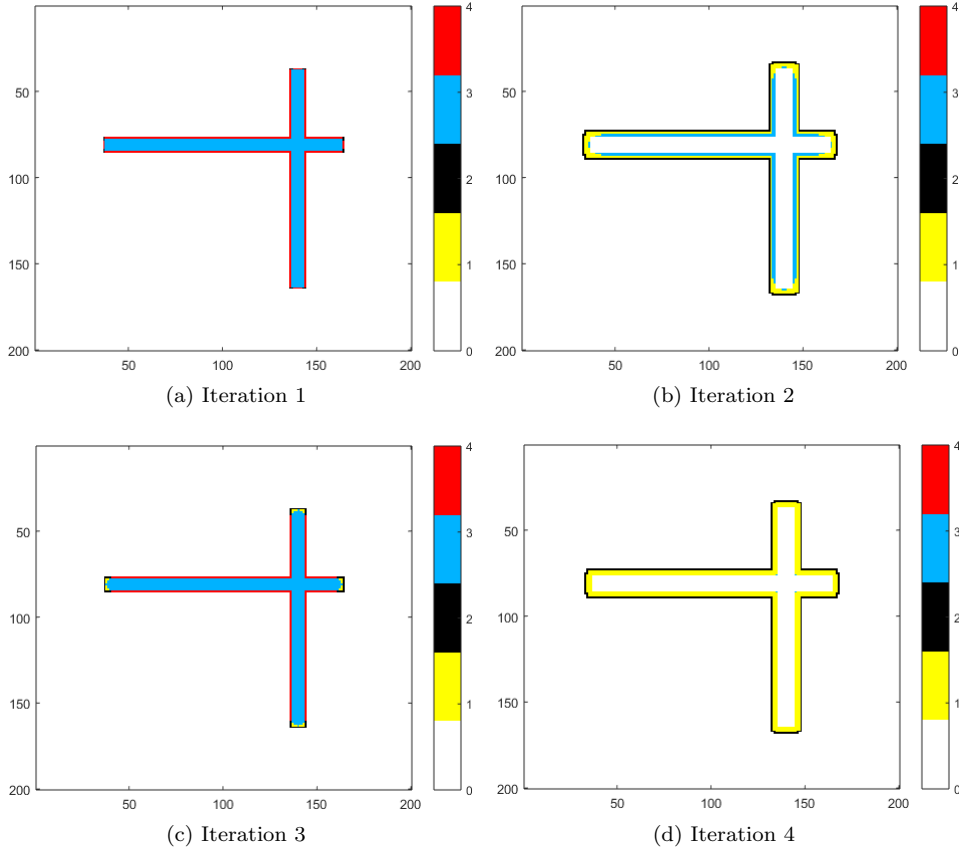


Figure 17: Flagging profiles for Case 2.1.

5.3.2. Case 2.2

The model from Case 2 is used. Computational performance of the case is summarized in Table 6. We plot the ratios of active domain (per timestep) versus simulation time in **Fig. 18**. We can see that the adaptive solver obtains an at least 11-fold reduction in solution effort, without degrading the original Newton convergence.

Table 6: Computational performance of Case 2.2.

	Timesteps	Total (inner) iterations	Total ratio M_A	Average ratio M_A per iteration
Adaptive Nonlinear DD	54	255	13.6	0.053
Standard Newton	54	153	153	1

This work develops a prototype algorithm for the adaptive DD solver, which can be further improved and optimized, e.g. exploiting the solution locality within each sub-

the flux across a cell interface. The method of choice for the time discretization is the fully-implicit scheme. The discrete form of conservation equation is given as,

$$\frac{V}{\Delta t} \left[(\phi \rho_T z_c)^{n+1} - (\phi \rho_T z_c)^n \right] - \sum_{ij} (x_c \rho_o F_o + y_c \rho_g F_g)^{n+1} - Q_c^{n+1} = 0. \quad (22)$$

where superscripts denote timesteps, and Δt is the timestep size. V is the cell volume. All indices related to the cell numeration are neglected. The accumulation term involves the total density,

$$\rho_T z_c = x_c \rho_o s_o + y_c \rho_g s_g \quad (23)$$

and,

$$\rho_T = \begin{cases} s_o \rho_o(\mathbf{x}) + s_g \rho_g(\mathbf{y}), & \text{two phase,} \\ \rho_l(\mathbf{z}), & \text{one phase.} \end{cases} \quad (24)$$

where $\rho_o(\mathbf{x})$ indicates the density computed at a composition \mathbf{x} , and $\rho_l(\mathbf{z})$ is the density computed in the single-phase regime at a composition \mathbf{z} .

The discrete phase flux across the interface (ij) between two cells is written as,

$$F_{l,ij} = \Upsilon_{ij} \lambda_{l,ij} \Delta \Phi_{l,ij} \quad (25)$$

where subscript (ij) denotes quantities defined at the cell interface. Υ_{ij} is the interface transmissibility. $\Delta \Phi_{l,ij} = \Delta p_{ij} - g_{l,ij}$ is the phase potential difference with the discrete weights $g_{l,ij} = \rho_{l,ij} g \Delta h_{ij}$. The phase and compositional coefficients associated with the flux terms are evaluated using the Phase-Potential Upwinding (PPU) scheme.

References

- [1] S.C. Maxwell, T.I. Urbancic, N. Steinsberger, R. Zinno, others, Microseismic imaging of hydraulic fracture complexity in the Barnett shale, in: SPE Annu. Tech. Conf. Exhib., 2002.
- [2] M.K. Fisher, C.A. Wright, B.M. Davidson, A.K. Goodwin, E.O. Fielder, W.S. Buckler, N.P. Steinsberger, others, Integrating fracture mapping technologies to optimize stimulations in the Barnett Shale, in: SPE Annu. Tech. Conf. Exhib., 2002.
- [3] M.J. Mayerhofer, E. Lonon, N.R. Warpinski, C.L. Cipolla, D.W. Walser, C.M. Rightmire, others, What is stimulated reservoir volume?, SPE Prod. Oper. 25 (2010) 89–98.
- [4] C.L. Cipolla, E.P. Lonon, J.C. Erdle, B. Rubin, others, Reservoir modeling in shale-gas reservoirs, SPE Reserv. Eval. Eng. 13 (2010) 638–653.
- [5] X. Weng, O. Kresse, D. Chuprakov, C.-E. Cohen, R. Prioul, U. Ganguly, Applying complex fracture model and integrated workflow in unconventional reservoirs, J. Pet. Sci. Eng. 124 (2014) 468–483.
- [6] C.L. Cipolla, N.R. Warpinski, M. Mayerhofer, E.P. Lonon, M. Vincent, others, The relationship between fracture complexity, reservoir properties, and fracture-treatment design, SPE Prod. Oper. 25 (2010) 438–452.
- [7] D.Y. Ding, Y.S. Wu, L. Jeannin, Efficient simulation of hydraulic fractured wells in unconventional reservoirs, J. Pet. Sci. Eng. 122 (2014) 631–642.
- [8] P. Panfili, R. Colin, A. Cominelli, D. Giamminonni, L. Guerra, others, Efficient and effective field scale simulation of hydraulic fractured wells: methodology and application, in: SPE Reserv. Characterisation Simul. Conf. Exhib., 2015.
- [9] M. Karimi-Fard, L.J. Durlofsky, K. Aziz, others, An efficient discrete fracture model applicable for general purpose reservoir simulators, in: SPE Reserv. Simul. Symp., 2003.
- [10] B.T. Mallison, M.-H. Hui, W. Narr, Practical gridding algorithms for discrete fracture modeling workflows, in: ECMOR XII-12th Eur. Conf. Math. Oil Recover., 2010: p. cp–163.

- [11] V. Artus, D. Fructus, Transmissibility corrections and grid control for shale gas numerical production forecasts, *Oil Gas Sci. Technol. d'IFP Energies Nouv.* 67 (2012) 805–821.
- [12] J. Jiang, R.M. Younis, Hybrid coupled discrete-fracture/matrix and multicontinuum models for unconventional-reservoir simulation, *SPE J.* 21 (2016).
- [13] M. HosseiniMehr, M. Cusini, C. Vuik, H. Hajibeygi, Algebraic dynamic multilevel method for embedded discrete fracture model (F-ADM), *J. Comput. Phys.* 373 (2018) 324–345.
- [14] X. Xue, A. Rey, P. Muron, G. Dufour, X.-H. Wen, others, Simplification and Simulation of Fracture Network Using Fast Marching Method and Spectral Clustering for Embedded Discrete Fracture Model, in: *SPE Hydraul. Fract. Technol. Conf. Exhib.*, 2019.
- [15] K. Pruess, T.N. Narasimhan, A practical method for modeling fluid and heat flow in fractured porous media, *Soc Petrol Eng J.* (1982).
- [16] J.E. Warren, P.J. Root, others, The behavior of naturally fractured reservoirs, *Soc. Pet. Eng. J.* 3 (1963) 245–255.
- [17] H. Kazemi, L.S. Merrill Jr, K.L. Porterfield, P.R. Zeman, others, Numerical simulation of water-oil flow in naturally fractured reservoirs, *Soc. Pet. Eng. J.* 16 (1976) 317–326.
- [18] M.-H. Hui, B.T. Mallison, M.H. Fyrozjaee, W. Narr, others, The upscaling of discrete fracture models for faster, coarse-scale simulations of IOR and EOR processes for fractured reservoirs, in: *SPE Annu. Tech. Conf. Exhib.*, 2013.
- [19] Y.-S. Wu, J. Li, D. Ding, C. Wang, Y. Di, others, A generalized framework model for the simulation of gas production in unconventional gas reservoirs, *Spe J.* 19 (2014) 845–857.
- [20] J. Jiang, R.M. Younis, A multimechanistic multicontinuum model for simulating shale gas reservoir with complex fractured system, *Fuel.* 161 (2015).
- [21] N. Farah, D.Y. Ding, Y.S. Wu, others, Simulation of the impact of fracturing fluid induced formation damage in shale gas reservoirs, in: *SPE Reserv. Simul. Symp.*, 2015.
- [22] G.T. Ren, J.M. Jiang, R.M. Younis, XFEM-EDFM-MINC for coupled geomechanics and flow in fractured reservoirs, in: *15th Eur. Conf. Math. Oil Recover. ECMOR 2016*, 2016.
- [23] D.Y. Ding, N. Farah, B. Bourbiaux, Y.-S. Wu, I. Mestiri, others, Simulation of matrix/fracture interaction in low-permeability fractured unconventional reservoirs, *SPE J.* 23 (2018) 1–389.
- [24] K. Aziz and A. Settari. *Petroleum reservoir simulation.* Chapman & Hall, 1979.
- [25] K. Coats, An equation of state compositional model, *SPE J.* 20(05) (1980) 363–376.
- [26] R. Younis, H.A. Tchelepi, K. Aziz, others, Adaptively Localized Continuation-Newton Method–Nonlinear Solvers That Converge All the Time, *SPE J.* 15 (2010) 526–544.
- [27] M. Cusini, C. van Kruijsdijk, H. Hajibeygi, Algebraic dynamic multilevel (ADM) method for fully implicit simulations of multiphase flow in porous media, *J. Comput. Phys.* 314 (2016) 60–79.
- [28] M. Cusini, B. Fryer, C. van Kruijsdijk, H. Hajibeygi, Algebraic dynamic multilevel method for compositional flow in heterogeneous porous media, *J. Comput. Phys.* 354 (2018) 593–612.
- [29] S.M. Sheth, R.M. Younis, others, Localized linear systems in sequential implicit simulation of two-phase flow and transport, *SPE J.* 22 (2017) 1–542.
- [30] P. Lu, B.L. Beckner, others, An adaptive Newton's method for reservoir simulation, in: *SPE Reserv. Simul. Symp.*, 2011.
- [31] J. Jiang, H.A. Tchelepi, Dissipation-based continuation method for multiphase flow in heterogeneous porous media, *J. Comput. Phys.* 375 (2018) 307–336.

- [32] D. V Voskov, H.A. Tchelepi, Comparison of nonlinear formulations for two-phase multi-component EoS based simulation, *J. Pet. Sci. Eng.* 82 (2012) 101–111.
- [33] M.L. Michelsen, The isothermal flash problem. Part I. Stability, *Fluid Phase Equilib.* 9 (1982) 1–19.
- [34] M.L. Michelsen, The isothermal flash problem. Part II. Phase-split calculation, *Fluid Phase Equilib.* 9 (1982) 21–40.
- [35] V. Dolean, M.J. Gander, W. Kheriji, F. Kwok, R. Masson, Nonlinear preconditioning: How to use a nonlinear Schwarz method to precondition Newton’s method, *SIAM J. Sci. Comput.* 38 (2016) A3357–A3380.
- [36] X.-C. Cai, W.D. Gropp, D.E. Keyes, R.G. Melvin, D.P. Young, Parallel Newton–Krylov–Schwarz algorithms for the transonic full potential equation, *SIAM J. Sci. Comput.* 19 (1998) 246–265.
- [37] J.O. Skogestad, E. Keilegavlen, J.M. Nordbotten, Domain decomposition strategies for nonlinear flow problems in porous media, *J. Comput. Phys.* 234 (2013) 439–451.
- [38] J. Jiang, H.A. Tchelepi, Nonlinear acceleration of sequential fully implicit (SFI) method for coupled flow and transport in porous media, *Comput. Methods Appl. Mech. Eng.* 352 (2019) 246–275.
- [39] S.H. Lee, M.F. Lough, C.L. Jensen, Hierarchical modeling of flow in naturally fractured formations with multiple length scales, *Water Resour. Res.* 37 (2001) 443–455.
- [40] L. Li, S.H. Lee, others, Efficient field-scale simulation of black oil in a naturally fractured reservoir through discrete fracture networks and homogenized media, *SPE Reserv. Eval. Eng.* 11 (2008) 750–758.
- [41] H. Hajibeygi, D. Karvounis, P. Jenny, A hierarchical fracture model for the iterative multiscale finite volume method, *J. Comput. Phys.* 230 (2011) 8729–8743.
- [42] A. Moinfar, A. Varavei, K. Sepehrnoori, R.T., Johns. Development of an Efficient Embedded Discrete Fracture Model for 3D Compositional Reservoir Simulation in Fractured Reservoirs, *SPE Journal*, 19(02), (2014) pp.289-303.
- [43] J. Jiang, R.M. Younis, An improved projection-based embedded discrete fracture model (pEDFM) for multiphase flow in fractured reservoirs, *Adv. Water Resour.* 109 (2017).
- [44] M. Tene, S.B.M. Bosma, M.S. Al Kobaisi, H. Hajibeygi, Projection-based embedded discrete fracture model (pEDFM), *Adv. Water Resour.* 105 (2017) 205–216.
- [45] G. Ren, J. Jiang, R.M. Younis, A Model for coupled geomechanics and multiphase flow in fractured porous media using embedded meshes, *Adv. Water Resour.* 122 (2018) 113–130.
- [46] M.-H. Hui, G. Dufour, S. Vitel, P. Muron, R. Tavakoli, M. Rousset, A. Rey, B. Mallison, others, A Robust Embedded Discrete Fracture Modeling Workflow for Simulating Complex Processes in Field-Scale Fractured Reservoirs, in: *SPE Reserv. Simul. Conf.*, 2019.
- [47] X. Xue, C. Yang, T. Onishi, M.J. King, A. Datta-Gupta, others, Modeling Hydraulically Fractured Shale Wells Using the Fast-Marching Method With Local Grid Refinements and an Embedded Discrete Fracture Model, *SPE J.* (2019).
- [48] A. Rey, J. Schembre, X.-H. Wen, others, Calibration of the Water Flowback in Unconventional Reservoirs with Complex Fractures using Embedded Discrete Fracture Model EDFM, in: *SPE Liq. Basins Conf. Am.*, 2019.
- [49] J. Lohrenz, B.G. Bray, C.R. Clark, others, Calculating viscosities of reservoir fluids from their compositions, *J. Pet. Technol.* 16 (1964) 1–171.